Nonlinear numerical modelling of FRP reinforced glued laminated timber

CrossMark

Gary M. Raftery [a], Annette M. Harte [b,*]

[a] Department of Civil and Environmental Engineering, Faculty of Engineering, The University of Auckland, New Zealand
[b] Civil Engineering, College of Engineering and Informatics, National University of Ireland, Galway, Ireland

ABSTRACT

Fibre-reinforced polymers (FRPs) are effective in the flexural stiffening and strengthening of structural members. Such systems can be optimised if accurate numerical models are developed. At present, limited information is available in the literature on numerical models that can predict with good accuracy the nonlinear behaviour of FRP reinforced low-grade glued laminated timber beams. This paper discusses the development of a finite element model, which incorporates nonlinear material modelling and nonlinear geometry to predict the load–deflection behaviour, stiffness, ultimate moment capacity and strain distribution of FRP plate reinforced glued laminated timber beams manufactured from mechanically stress graded spruce. Beams with and without sacrificial laminations are modelled and their performance is compared to unreinforced glued laminated timber beams. The model employed anisotropic plasticity theory for the timber in compression. The failure model used was the maximum stress criterion. Strong agreement was obtained between the predicted behaviour and the associated experimental findings. It was deduced from comparing the results from the numerical model with experimental findings that the FRP plate succeeds in increasing the performance of the adjacent timber significantly. The model is a useful tool for examination of the effect of reinforcement percentage and will be used for optimisation of the hybrid beam.

© 2013 Elsevier Ltd. All rights reserved.

1. General Introduction

Fibre reinforced materials (FRPs) comprise a class of advanced composite materials whereby in recent years structural engineers are gaining greater awareness of the numerous advantages that these materials can offer in the construction industry [1,2]. Primary emphasis has been on the strengthening and rehabilitation of concrete structural elements with limited work undertaken in the reinforcement of timber. Timber is a renowned traditional building material, a natural renewable material, cost competitive, recyclable and aesthetically pleasing [3,4]. It has a negative carbon output and therefore it makes both economic and environmental sense to promote its use in the construction sector. FRP materials are an ideal reinforcement for timber because of their high stiffness and high strength to weight ratio. Furthermore, superior durability is portrayed by these materials in corrosive environments in addition to the excellent fatigue resistance that they possess. Experimental research has shown that by strategically locating FRP plate material in the higher stressed tensile zone of low-grade glued

laminated timber (glulam) beams, significant improvements in the strength of the members as well as modest improvements in the stiffness can be achieved [5]. Furthermore, the FRP reinforced beams are associated with more ductile behaviour in comparison to the linear elastic brittle tensile failures that are experienced by the unreinforced glulam. Plate reinforcement is more compatible with the glulam manufacturing process than rod reinforcement. A comprehensive review of previous experimental research undertaken using FRP materials to reinforce timber is presented in [5]. However, considerable costs are associated with experimental testing programmes. Numerical modelling is an effective tool which can be used to optimise the performance of structural elements such as FRP reinforced glulam. If experimental behaviour can be simulated to a satisfactory level of precision, further analyses of the reinforced beams can be studied using a numerical approach. The costs that would be associated with extensive test programmes can therefore be significantly reduced. This paper discusses the development of a numerical model that formed part of a larger study carried out to investigate the use of FRP plates to reinforce glulams manufactured with low-grade Irish Sitka spruce [6]. The model incorporates both material and geometric nonlinearities and is used to predict the load–deflection behaviour, stiffness, ultimate moment capacity and strain distribution of FRP plate

* Corresponding author. Tel.: +353 91 492732.
E-mail addresses: g.raftery@auckland.ac.nz (G.M. Raftery), annette.harte@nui-galway.ie (A.M. Harte).

reinforced glulam beams manufactured from mechanically stress graded spruce. Model validation against the results of experimental testing is presented.

1.1. Previous studies which involved numerical modelling of timber and FRPs

Timber is a complex material to model because of the anisotropic behaviour it exhibits as well as the variability that exists in the material as a result of the high number of defects that are randomly present. This is further complicated by its inherent nonlinear characteristics in compression. A number of previous studies have been undertaken where numerical models have been developed to examine the behaviour of composites of timber and FRP. However, limited literature exists on the development of finite element models where nonlinear material modelling of the timber is included. A two dimensional finite element model was developed by Tingley [7] to examine the stress–strain relationship of FRP reinforced glulam. However, plasticity was not considered in the model. Good agreement was obtained between the actual bending stresses obtained from experimental investigation and the model. Kirlin used a linear model to examine the stress concentrations at the end of the reinforcement in partially reinforced FRP-glulam beams [8]. The stress concentrations were seen to be greatly influenced by the FRP thickness and stiffness. Serrano developed a nonlinear three-dimensional bond-line model to examine the behaviour of glued-in rods for timber structures. There was no requirement to include a plastic material model for the timber in the model and therefore the timber was modelled as a linear elastic orthotropic material [9]. Kasal and Heiduschke used a three dimensional finite element model to analyse the use of composite materials in the radial reinforcement of curved glulam [10]. It is not clear if a material model that includes plasticity is included for the timber. The predicted strains were found to be in good agreement with those determined from the experimental testing. Glulam which was pre-stressed with GFRP was modelled in another study. The material model for the timber comprised an orthotropic elastic model. Good correlation was obtained with the experimental results although little ductility was associated with the tested beam [11]. Alam employed anisotropic plasticity in a three dimensional model to predict with good accuracy the proportional limit of laminated veneer lumber beams reinforced with bonded-in fibre reinforced polymers [12]. No predictions of the strain profile distribution or of failure were included in the study. Kim and Harries reported on the development of a three-dimensional model which predicted with good accuracy the linear elastic behaviour to failure of CFRP reinforced timber beams [13]. A further study developed an approach for modelling the nonlinear behaviour of reinforced solid timber sections [14]. The authors found that the bond shear-slip between FRP reinforcement and timber had little effect on the stiffness and ultimate load capacity of the reinforced beams and that the assumption of a perfect bond between the FRP and timber was acceptable in the model.

1.2. Objectives of the present study

The objective of this study was to develop a nonlinear numerical model that could accurately simulate the mechanical behaviour of unreinforced and FRP reinforced low-grade glulam during static loading. Accurate predictions of load–deflection behaviour, flexural stiffness, ultimate moment capacity and strain profile distribution are required in order to facilitate optimisation of the hybrid system.

2. Development of the FRP reinforced glulam numerical model

2.1. Experimental arrangement to be simulated

Finite element modelling was carried out for all of the beam configurations used in the experimental programme. This necessitated the development of numerical models for unreinforced glulam beams (Phase A; 190 mm deep), FRP plate reinforced glulam beams (Phase B; 190 mm deep), unreinforced glulam beams (Phase C; 215 mm deep) and FRP plate reinforced glulam beams which included a sacrificial lamination (Phase D; 215 mm deep). The beam test set-up as specified in EN408 [15] is shown in Fig. 1 and the beam configurations are shown in Fig. 2. All dimensions shown in the figures throughout the paper are in millimetres. The glulam beams were manufactured from mechanically graded C16 Sitka spruce laminations and the arrangement of the laminations was optimised such that better quality material was located in higher stressed zones. Each glulam beam comprised five laminations 96 mm in width and 38 mm in thickness which were bonded together using a phenol resorcinol formaldeyhyde (PRF) adhesive to produce a section 96 mm wide and 190 mm deep. The Phase B reinforced beams had an FRP plate bonded to the soffit of the glulam with an epoxy adhesive (Sikadur 31) after the thickness of the bond-line and reinforcement plate was planed from the timber so that a performance comparison could be obtained with the unreinforced beams. The addition of a 25 mm thick sacrificial lamination was examined in the Phase C unreinforced beams and in the FRP plate reinforced glulam beams in Phase D. The FRP reinforcement comprised unidirectional glass-fibres in an engineered thermoplastic polyurethane matrix (Fulcrum). Two 1.2 mm thick FRP plates were adhesively bonded together to form a plate 96 mm in width and 2.8 mm in thickness. Data from strain gauges placed on one of the beams, using the arrangement illustrated in Fig. 3, enabled comparisons between the numerical and experimental strain distributions.

2.2. Development of the nonlinear numerical model

2.2.1. Model geometry and boundary constraints

The commercial finite element package, ANSYS, was used to generate a two-dimensional plane stress model for the experimentally tested beams. Because of the symmetrical arrangement of the test set-up, it was only necessary to model half of the beam as shown in Fig. 4.
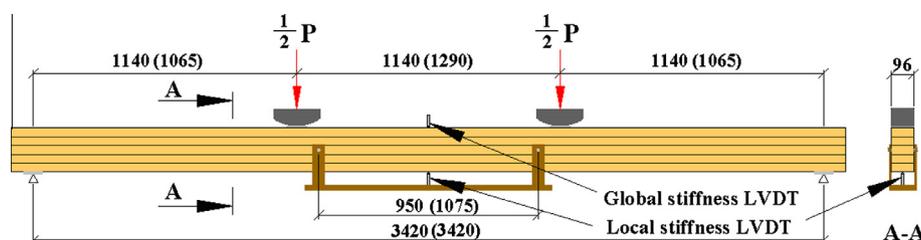

Fig. 1. Stiffness test arrangement for Phase A and Phase B beams. (arrangement for Phase C and Phase D beams shown in brackets).
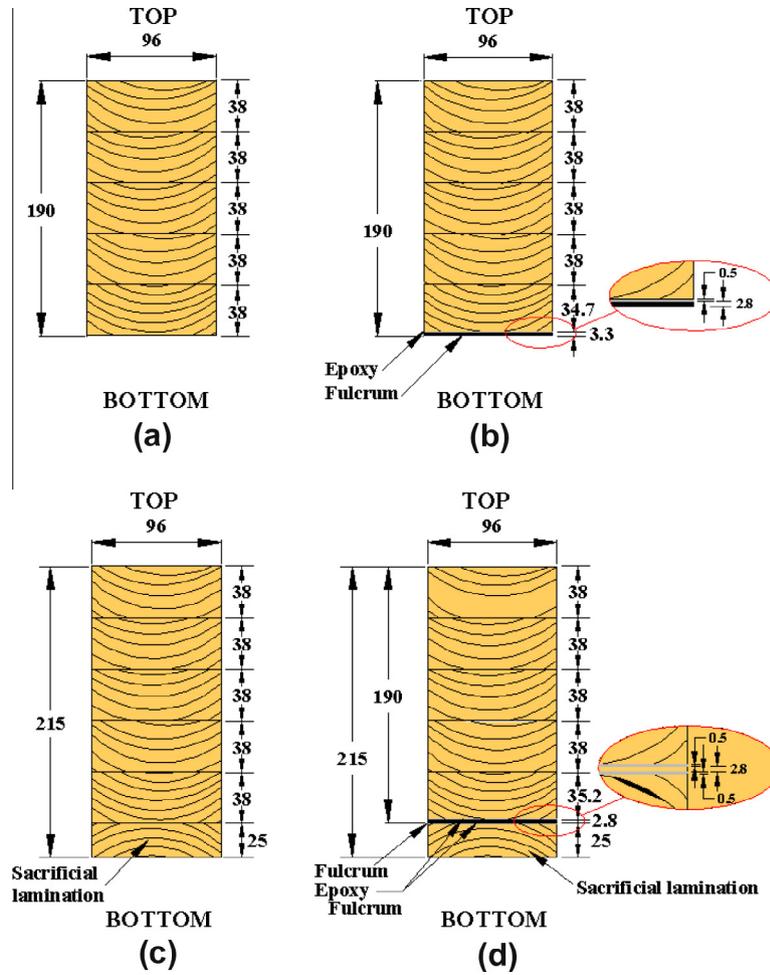
Fig. 2. Beam configurations: (a) Phase A, (b) Phase B, (c) Phase C, and (d) Phase D.

Each lamination was modelled as a separate entity. This procedure allowed the material characteristics of each lamination to be modelled individually. A perfect bonded connection was assumed to exist at the PRF bonded interface between the laminations as there was no evidence of premature bond-line failures in the glulam beams during testing. The PRF adhesive had also achieved excellent results with the timber in previous studies [16,17]. The PRF adhesive layer was not included in the model as its thickness was in the range of 0.1 mm. A perfect bonded connection was also assumed to exist at the epoxy/wood interface and the epoxy/FRP interface as failure occurred in the timber of the bottom tension lamination when testing both the unreinforced and reinforced beams with no evidence of failure at these interfaces [5]. Furthermore, bonds of very high quality were obtained between the Sikadur 31 epoxy adhesive, the FRP type and the wood in a previous experimental study [18]. As a result no interface elements were required and it was not required to model slip behaviour as the cohesive strength of the epoxy was greater than the cohesive strength of the wood. The perfect bonds were therefore modelled such that adjacent entities were associated with common boundaries. The model also replicated the experimental test set-up by including 100 mm long steel plates, which were placed at the loading and support points in order to avoid stress concentrations at these
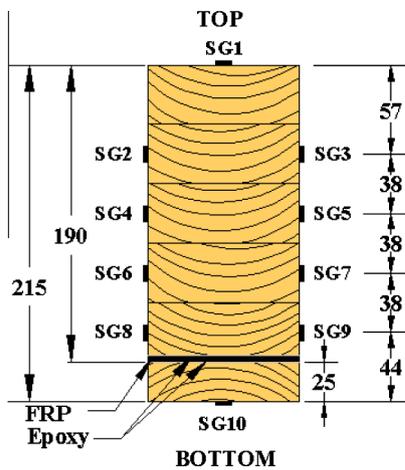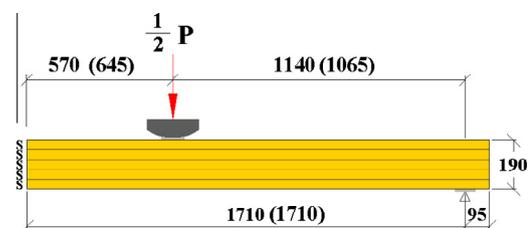

Fig. 3. Strain gauge arrangements (Beam 21).

Fig. 4. Geometrical arrangement of FE model for Phase A and Phase B beams. (arrangement for Phase C and Phase D beams shown in brackets).
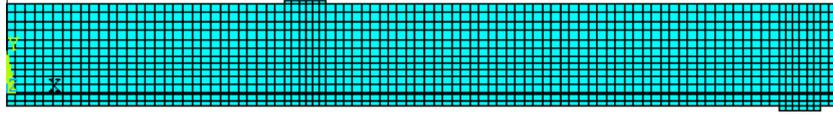
Fig. 5. Mesh discretisation for Phase D beams.

locations. No slip was included at the interface between the steel plates and wood surface as no slip was experienced during the experimental testing. Second order plane stress elements were used for the meshing in the model. The mesh density shown in Fig. 5 for modelling the Phase D beams was selected based on the accuracy of the model and available computational power [6]. A roller support condition which restrained the beam from displacing in the direction perpendicular to the beam axis was used to define the constraint condition at the support located at 95 mm from the end of the beam.

2.2.2. Material models

The use of a suitable constitutive model for each defined material is imperative if the model is to accurately predict the structural performance of the hybrid beam. Little ductility is generally experienced by unreinforced glulam beams when a balanced lay-up is used and a linear model is usually appropriate for such an arrangement. When even small percentages of tensile reinforcement are added to glulam, nonlinear behaviour can be introduced. In this case, a linear elastic, perfectly plastic material model was employed to model the behaviour of the timber parallel to grain in compression while a linear elastic brittle material model is employed for timber in tension as determined from in-grade uniaxial experimental test programmes [6,19]. The behaviour is illustrated in Fig. 6. The ultimate tensile strength, σ_{Lu}^t occurs at a strain, ε_{Lu}^t. The ultimate compressive strength σ_{Ly}^c occurs at a strain, ε_{Ly}^c and perfect plastic behaviour occurs in the longitudinal direction of the timber after this strain value. The tensile stress along the longitudinal axis is represented by σ_L^t and the compressive stress along the longitudinal axis is represented by σ_L^c.

ANSYS includes material models based on the theory of anisotropic plasticity [20] and this theory was used in this study to account for the plastic behaviour of the material in the compression zone. The theory is based upon the yield criterion by Hill [21]. Shih and Lee [22] added to the theory to accommodate differences in the tensile and compressive yield strengths in the orthotropic material. It requires that two criteria must be satisfied. Plastic incompressibility must be satisfied. This means that there is no volume change during plastic straining. The second criterion requires that a closed yield surface, that is elliptical in cross section, is maintained. While nine constants are required for orthotropic
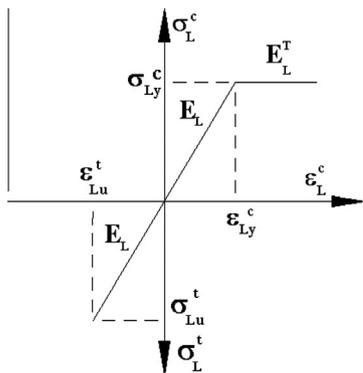
elastic materials, an additional 18 are required so that anisotropic plasticity theory can be applied correctly in this model. The selection of a full set of yield stresses and tangent moduli to satisfy the criteria is particularly challenging for materials, such as timber, which have a high level of orthotropy in their properties. Bi-linear behaviour for the timber in the three orthogonal directions as well as the three shear planes is included in the model. This means that normal compressive yield stresses are declared for the longitudinal, σ_{Ly}^c, radial, σ_{Ry}^c and tangential, σ_{Ty}^c directions as well as yield shear stresses in the three planes. The behaviour of the material after yielding is defined by tangent moduli, E^T, or tangent shear moduli, G^T. The elastic–plastic responses for the timber in compression in the radial and tangential directions are shown in Fig. 7a and b, respectively. Characterisation of the materials is discussed in Section 3. Characterisation of the other materials is less complex. A linear elastic orthotropic material model was used for the characterisation of the FRP plate. Linear elastic isotropic material models were used for the epoxy adhesive and the steel loading plates.

Execution of the model involved a static small displacement analysis, whereby a series of displacement-controlled increments were applied at the loading plate during which convergence was obtained. The displacement at midspan and the corresponding reaction force were recorded for every increment. Failure in the
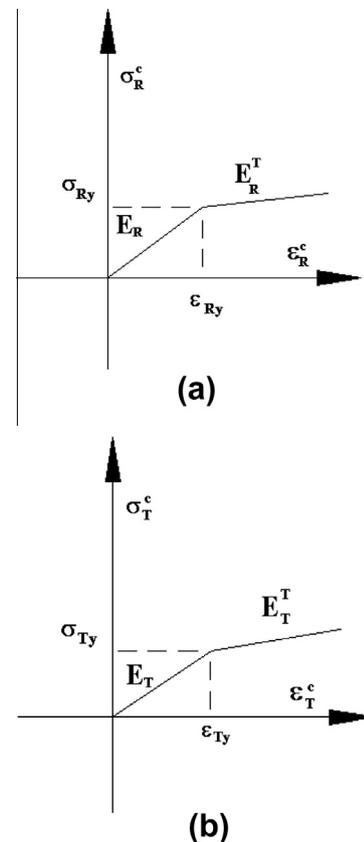

(a)

(b)

Fig. 7. Elastic–plastic stress–strain relationships in compression (a) radial direction (b) tangential direction.

Fig. 6. Elastic–plastic stress–strain behaviour of timber parallel to grain.

Table 1
Modelling and experimental test programmes.

Phase	Arrangement	Depth (mm)	Repetitions	Beam numbers tested and modelled
A	Unreinforced glulam	190	6	1, 2, 3, 36, 37, 38
B	Reinforced glulam	190	5	5, 11, 18, 24, 31
C	Unreinforced glulam	215	10	4, 9, 10, 16, 17, 22, 23, 29, 30, 33
D	Reinforced glulam	215	5	8, 15, 21[a], 28, 35

[a] Includes modelling of strain profile behaviour.

model was based on the maximum stress criterion whereby the model was programmed to deactivate elements when the tensile stresses in the longitudinal direction, at a displacement step, reached the critical tensile failure stresses of the timber laminations.

2.3. Modelling programme

The beam testing series from [5] and beam numbers which were modelled are clearly stated in Table 1. All beams tested were modelled. For the beams which included the reinforcement in the test programme, modelling was carried out to assess the performance of these beams in relation to both ultimate moment capacity and stiffness in both their reinforced and unreinforced state. Strain profiles between experimental and numerical results were compared for Beam 21 (Phase D). An examination was also undertaken to assess the mechanical performance of the reinforced beams if critical strength reducing defects were removed from the bottom tension lamination.

3. Material characterisation

The material characterisation, which was used for the input to the model, involved experimental testing, the determination of properties from previously established relationships and the use of published data available in the literature.

3.1. FRP properties

The FRP material was tested in tension with reference to EN 2747 [23] in order to determine its tensile modulus of elasticity and tensile strength. Tests were carried out on 1.2 mm thick FRP plate and 2.8 mm thick FRP plate (two plates of 1.2 mm bonded together with epoxy adhesive) as used for the FRP reinforcement of low-grade glulam beams [5]. Ten repetitions were executed for the 1.2 mm plate and nine repetitions were undertaken for the 2.8 mm plate. The 1.2 mm plate was not strength tested. The FRP material specimens were manufactured according to unidirectional thermoplastic specimen Type 1. Hardboard tabs were bonded to the ends of the specimens so that slipping at the grips would be prevented during testing. Furthermore, these tabs helped to reduce stress concentrations at the grips. The cross-sectional areas of the specimens were measured prior to testing using a vernier caliper with precision to 0.01 mm. After ensuring perfect vertical placement of the specimens in the tension testing machine as shown in Fig. 8, the specimen was clamped uniformly in the grips and an extensometer with 50 mm gauge length was fitted to the tensile specimens prior to testing at a displacement speed of 0.033 mm/s. Testing was executed using a 250 kN Denison testing machine and tests were only carried out when conditions of 65 ± 5% relative humidity and temperature of 20 ± 2 °C were present in the laboratory.

The tensile modulus of elasticity of the FRP plate was determined to be 40,110 N/mm^2 with a standard deviation of 1,190 N/mm^2. When two 1.2 mm thick Fulcrum pieces were bonded
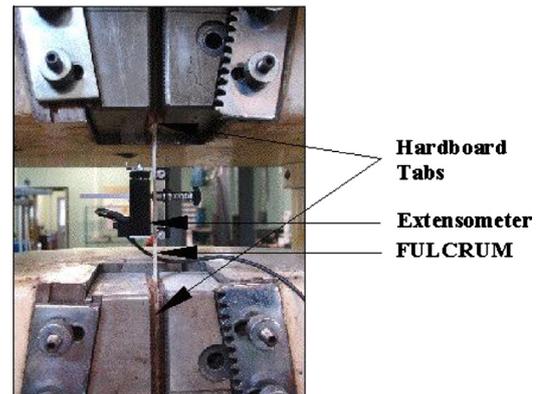
Fig. 8. FRP tensile test.

Table 2
Properties used for FRP during finite element modelling.

E_1	38.44	GPa
E_2	6.34	GPa
E_3	6.34	GPa
G_{12}	1.9	GPa
v_{12}	0.24	
v_{21}	0.05	

together with a thin epoxy bond-line of 0.4 mm, a mean modulus of elasticity of 38,440 N/mm^2 with standard deviation of 2,250 N/mm^2 was determined. The mean tensile strength of the two plates bonded together was determined to be 701 N/mm^2 with a standard deviation of 45 N/mm^2. This was the arrangement that was used for the reinforcement in the experimental test programme as described in [5]. The value of 38,440 N/mm^2 was therefore used in the numerical model. The test values are lower than the values stated by the manufacturer because the presence of the epoxy layer between the two plates results in a lower overall fibre volume fraction than a single plate. A summary of the mechanical properties used in the modelling for the FRP is presented in Table 2.

The transverse modulus of elasticity E_2 was calculated from the inverse rule of mixtures as stated in Eq. (1), assuming a solid plate was used during the testing. The fibre volume fraction, V_f and matrix volume fraction, V_m were back-calculated using the rule of mixtures and the average Young's modulus value determined from the mechanically tested specimens. The values used for the Young's modulus of the glass fibres, E_f and Young's modulus of the matrix, E_m were taken from the literature [2]. The in plane shear modulus was determined from Eq. (2) where G_f and G_m are the shear moduli of the glass fibre and matrix materials, respectively. Poisson's ratio, v_{12} and v_{21} are approximated using Eqs. (3) and (4), where v_f is Poisson's ratio of the glass fibres and v_m is Poisson's ratio of the matrix. Values stated in the literature were used to estimate the properties of the material [1,2,24]

$$E_2 = \frac{E_f E_m}{E_f V_m + E_m V_f} \tag{1}$$

$$G_{12} = \frac{G_f G_m}{G_f V_m + G_m V_f} \quad (2)$$

$$v_{12} = v_f V_f + v_m V_m \quad (3)$$

$$v_{21} = \frac{E_2}{E_1} v_{12} \quad (4)$$

3.2. Timber properties

The global bending modulus of elasticity of each timber lamination was determined by applying the central difference technique to the modulus of elasticity readings, which were determined at 100 mm intervals along each board during the mechanical stress grading procedure [6]. The general relationships as expressed in the literature [25] for the Young's moduli in the three timber orientations as shown in Eq. (5) and the relationship between the three shear moduli as shown in Eq. (6) were used for the timber and applied in the model

$$E_L : E_R : E_T \approx 20 : 1.6 : 1 \quad (5)$$

$$G_{LR} : G_{LT} : G_{RT} \approx 10 : 9.4 : 1 \quad (6)$$

where E_L, E_R, E_T are the Young's moduli in the longitudinal, radial and tangential directions and G_{LR}, G_{LT}, G_{RT} are the shear moduli in the respective planes. The relationship between E_L and G_{LR} as expressed in Eq. (7) [25] was also used.

$$E_L : G_{LR} \approx 14 : 1 \quad (7)$$

Poisson's ratio values of 0.37, 0.47 and 0.43 for v_{LR}, v_{LT} and v_{RT}, respectively, were employed in the finite element model as given for Sitka spruce [4]. The relationships and sources of data used for the moduli of elasticity E, tangent moduli E^T, and the yield stresses f_y, in the three orthogonal directions are shown in Table 3. Axes orientation is illustrated in relation to the grain direction in the timber. A test programme of in-grade compression tests was undertaken and a relationship which was statistically significant was established to estimate the compressive yield stress of the timber based on the knot area ratio and wood density of each specimen [6]. The ultimate tensile strength in the longitudinal direction

Table 3
Elastic–plastic properties of the timber in compression for the three orthogonal axes.

Axes	E (N/mm$^2 \times 10^3$)	E^T (N/mm$^2 \times 10^3$)	σ_y (N/mm^2)
L	[a]	0	[b]
R	[c]	30 [d]	5.3 [d]
T	[c]	25 [d]	5.6 [d]

Key:
a. Mechanical stress grading results.
b. Material characterisation testing [6].
c. Eq. (5) Ref. [25].
d. Ref. [12]

Table 4
Elastic–plastic properties of the timber in compression for the three shear planes.

Axes	G (N/mm$^2 \times 10^3$)	G^T (N/mm$^2 \times 10^3$)	τ_y (N/mm^2)
LR	[e]	0 [d]	11 [d]
RT	[f]	0 [d]	11 [d]
LT	[f]	0 [d]	8 [d]

Key:
d. Ref. [12].
e. Eq. (7) Ref. [25].
f. Eq. (6) Ref. [25].

was determined from a relationship established based on the knot area ratio in the spruce [6]. The laminating effect, λ which is the increase in strength of a timber lamination when bonded in a glulam beam in comparison to when tested in a uniaxial test was accounted for prior to entering the failure strength data for the timber into the nonlinear numerical model code. Falk and Colling [26] reported a value of 1.26 for the laminating effect for a beam made of homogeneous C30 grade laminations. Use of higher grade C37 laminations resulted in a significantly lower laminating factors. Hence, the application of 1.26 to the tensile strength of the C16 grade laminations in this study is conservative. Elastic–plastic stress–strain data was also inputted for the three shear planes as shown in Table 4.

4. Results and discussion

The results from the finite element model for predictions of load–deflection behaviour, stiffness, ultimate moment capacity and strain profile distribution are discussed in the following sections.

4.1. Prediction of load–deflection behaviour

4.1.1. Phase A: unreinforced 190 mm deep beams
The load–deflection behaviour of the experimentally tested Phase A beams and predictions from the finite element model were compared and a typical example is shown in Fig. 9. Good agreement is obtained, with the predicted behaviour exhibiting linear elastic behaviour to failure which replicates the behaviour of the experimentally tested unreinforced beams. These unreinforced beams exhibited little plastic behaviour as timber with defects has a lower tensile strength than compressive strength [27]. Therefore, even when using better quality laminations at the bottom of the beam than at the top of the beam, the yield stress in tension is generally exceeded before the yield stress in compression is reached. The unreinforced beams thereby failed in tension in a brittle manner and the simulated behaviour replicated this failure mode.

4.1.2. Phase B: reinforced 190 mm deep beams
Predicted load–deflection behaviour from the finite element model is contrasted with the experimentally determined load–deflection behaviour for the Phase B beams with typical comparisons shown in Figs. 10 and 11. For each of the beams in Phase B, simulations are undertaken to predict the behaviour of the beam in its unreinforced condition (Phase A) and the behaviour when failure occurs at the in-grade strength of the bottom tension lamination when reinforced with an FRP plate (Phase B(i)). In general, good agreement is obtained in both the linear elastic range and in
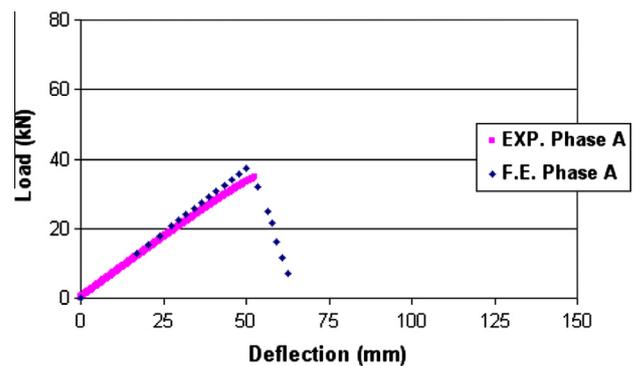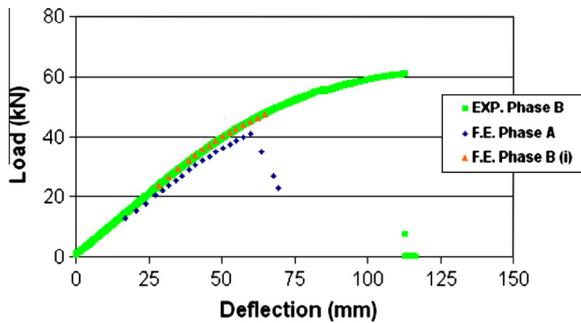

Fig. 9. Phase A: Beam 3, load–deflection behaviour.
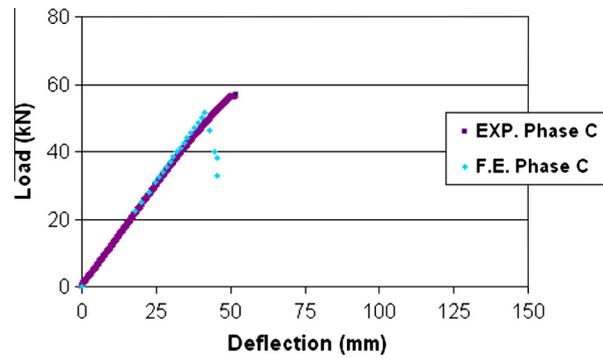
Fig. 10. Phase B: Beam 5, load–deflection behaviour.

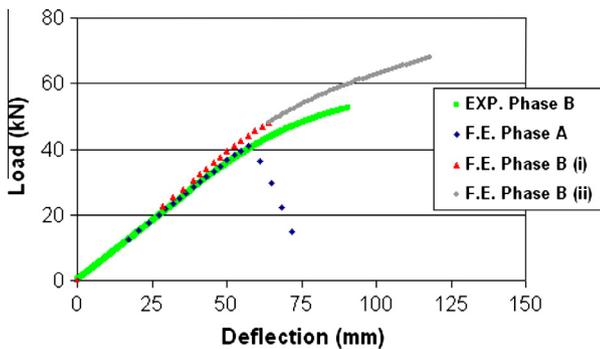**Fig. 12.** Phase C: Beam 9, load–deflection behaviour.

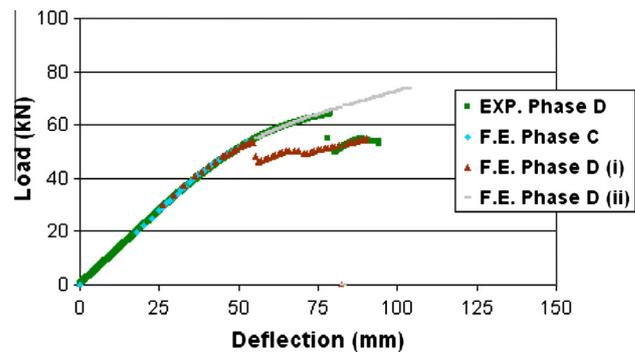**Fig. 11.** Phase B: Beam 18, load–deflection behaviour.

Fig. 13. Phase D: Beam 35, load–deflection behaviour.

the nonlinear region between the numerical predictions and experimental results. The experimental beams generally failed in the tension zone after compression wrinkling was experienced in the top lamination and the finite element model replicated these developments. The effect of improving the quality of the bottom timber lamination in the beam when also including the reinforcement, was examined by simulating the behaviour of Beam 18 using the maximum strength value for this timber, which corresponds to the strength of clear wood with no defects. This response is shown by the load–deflection curve labelled 'F.E. Phase B(ii)' in Fig. 11. The results from the model illustrate the extended nonlinear behaviour that can be achieved, hence highlighting the importance of eliminating significant defects from the more highly stressed tension zone.

4.1.3. Phase C: unreinforced 215 mm deep beams

A typical plot of the load–deflection behaviour from the experimental testing of the Phase C beams and the predicted load–deflection from the finite element model is shown in Fig. 12. In general, good agreement is obtained between the simulation and the experimental behaviour. All of the beams demonstrated linear elastic load–deflection behaviour to failure during testing and failure occurred in a brittle tensile manner, usually initiating within the zone of maximum bending moment. The failure mode predicted by the numerical model showed good agreement with this behaviour.

4.1.4. Phase D: reinforced 215 mm deep beams

The flexural performance of the five experimentally tested Phase D beams which included 1.12% FRP plate reinforcement and a sacrificial lamination is contrasted with the simulated behaviour predicted by the finite element model for an unreinforced beam of similar depth and identical mechanical properties (Phase C). The behaviour is also compared with that of a reinforced beam

where failure was predicted based on the strengths associated with the most significant knot area ratio in the sacrificial lamination and bottom tension lamination (Phase D(i)). A typical comparison is shown in Fig. 13. Good agreement is generally achieved between the experimental values and the predicted values with the numerical model predicting the nonlinear behaviour of the reinforced beams with good satisfaction. The results illustrate that the model has the ability to predict the drop in the load carrying capacity of the reinforced beams and the ability of the beams to carry load after failure has occurred in the sacrificial lamination. The model is conservative in comparison to the experimental behaviour when predicting this drop in load carrying capacity and is conservative in predicting the nonlinear behaviour that is associated with these reinforced beams. Simulations are also undertaken for a reinforced beam where the input failure strength is that of the clear wood of the sacrificial lamination in tension and the clear wood of the tension lamination above the FRP plate (Phase D(ii)) rather than failure being initiated at a knot. It is seen from a typical simulation shown in Fig. 13 that considerable nonlinear behaviour can be achieved if the quality of the most extremely stressed tension lamination is improved through a process such as finger-jointing.

4.2. Predictions of stiffness

The predictions of elastic stiffness obtained from the model are compared with the experimentally determined results in Table 5. Mean and coefficient of variation values are given. The experimental results for Phase A and Phase C unreinforced beams comprise the mean of a number of stiffness tests. The numerical model on average overpredicts the stiffness of the unreinforced beams and the reinforced beams but is within an acceptable range. Indentation at the supports in the global stiffness test and the variability associated with the mechanical stress grading machine are believed to be reasons for the differences between numerical

Table 5
Experimental versus predicted stiffness values.

Beam phase	Experimental EI (N/mm²)	Predicted EI (N/mm²)	Experimental EI/predicted EI
Phase A	4.98E+11 (0.08)	5.34E+10 (0.05)	0.93 (0.05)
Phase B	5.68E+11 (0.03)	5.74E+11 (0.02)	0.99 (0.04)
Phase C	7.06E+11 (0.11)	7.50E+11 (0.12)	0.94 (0.05)
Phase D	7.73E+11 (0.04)	8.00E+11 (0.02)	0.97 (0.04)

Note: coefficient of variation shown in brackets.

Table 6
Predicted stiffness of reinforced versus unreinforced beams.

Beam phase	Predicted EI of reinforced section (N mm²)	Predicted EI of equivalent unreinforced section (N mm²)	Percentage increase (%)
Phase B	5.74E+11 (0.02)	5.29E+11 (0.02)	8.4 (0.21)
Phase D	8.00E+11 (0.02)	7.73E+11 (0.01)	3.5 (0.32)

Note: coefficient of variation shown in brackets.

predictions and the global stiffness results. The differences are not overly significant and a good indication of the stiffness of each beam is obtained. The predictions of stiffness for glulam both with and without the reinforcement are compared in Table 6. The model predicted a mean increase of 8.4% stiffness if a 1.26% reinforcement percentage was added to the soffit of the beam. This is in contrast to a mean increase of 12.13% which was achieved in the experimental testing [5]. The predictions of stiffness for the Phase D beams, which included the FRP plate reinforcement above the sacrificial lamination, were also contrasted with predictions for unreinforced beams having laminations of the same mechanical characteristics. The finite element model predicted a mean increase in stiffness of 3.5%. This is in contrast to a mean increase of 7.4% which was achieved during the experimental testing (Table 5). These results appear to suggest that the FRP plate succeeds in improving the stiffness performance of the timber laminations adjacent to the FRP plate, which in turn improves the overall stiffness performance of the section.

4.3. Predictions of ultimate moment capacity

The predictions of ultimate moment capacity are contrasted with results from the experimental test programme in Table 7. Mean and coefficient of variation values are given. In general, the predictions are satisfactorily conservative and are considerably more accurate than the linear theoretical model presented in [5]. Deviations between the results are deemed to be as a result of the laminating factor being significantly greater for glulam fabricated from C16 spruce than the value which was used in the model. The value used corresponded to C30 grade spruce. Another possible reason for deviations is the low correlation coefficient of 0.3867 between the tensile strength of the timber and the knot area ratio as determined during the in-grade tension testing

Table 7
Experimental versus predicted ultimate moment capacities.

Beam phase	Experimental M_{ult} (kN m)	Predicted M_{ult} (kN m)	Experimental M_{ult}/predicted M_{ult}
Phase A	21.71 (0.08)	19.54 (0.09)	1.12 (0.19)
Phase B	29.96 (0.12)	26.14 (0.08)	1.14 (0.07)
Phase C	25.61 (0.14)	24.77 (0.09)	1.03 (0.08)
Phase D	32.93 (0.09)	27.66 (0.11)	1.19 (0.04)

Note: coefficient of variation shown in brackets.

Table 8
Predicted ultimate moment capacities of reinforced versus unreinforced beams.

Beam phase	Predicted M_{ult} of reinforced beams: (kN m)	Predicted M_{ult} of reinforced beams in unreinforced state: (kN m)	Percentage increase (%)
Phase B	26.14 (2.08)	22.33 (1.51)	17.0 (2.5)
Phase D	27.66 (2.94)	26.10 (2.62)	6.0 (1.8)

Note: coefficient of variation shown in brackets.

programme [6,19]. With a more intensive in-grade tension testing programme, it is thought that a higher correlation coefficient could be established which would increase the accuracy of the predictions outputted by the finite element model. Further accuracy could also be obtained if the model also accounted for margin knot area ratio (MKAR) where failure sometimes occurred during the experimental testing [5] rather than accounting solely for the total knot area ratio (KAR).

Comparisons in relation to ultimate moment capacity for the reinforced beams and unreinforced beams which were associated with laminations of the same mechanical properties were undertaken and the results are presented in Table 8. For the Phase B beams, the model predicts a mean increase in ultimate moment capacity of 17% in comparison to unreinforced beams having laminations of the same mechanical properties (Phase A). When the FRP reinforcement and sacrificial lamination is included (Phase D), the mean increase in ultimate moment capacity is 6% in comparison to beams with laminations of the same mechanical properties (Phase C). This contrasts with a 38% increase in ultimate moment capacity between Phase B and Phase A beams in the experimental test programme and a 28.6% increase in ultimate moment capacity between Phase D and Phase C beams. While it is noted that the quality of the laminations vary between the reinforced and unreinforced beams in the experimental test programme, it is also evident from these findings that the addition of the FRP plate succeeds in increasing the performance of the adjacent timber in relation to ultimate moment capacity of the reinforced element and assists in dissipating the stresses away from critical strength reducing defects such as knots.

Significant enhancements in the ultimate moment capacity can be achieved if premature failure of the most highly stressed tension lamination is prevented. This is demonstrated in the case of Beam 18 as shown in Fig. 11 for the Phase B beams where the finite element model predicted the mechanical behaviour of the reinforced beam up to the failure strength associated with the clear wood in the bottom tension lamination (F.E. Phase B(ii)). It was determined that an increase in the ultimate moment capacity of 65.2% could be achieved if failure was associated with the clear wood of the bottom lamination. Substantial enhancements can also be achieved in the reinforced beams of Phase D if premature failure at a knot is prevented as illustrated in Fig. 13.

4.4. Prediction of strain profile

The strain profile distributions predicted by the numerical model when failure is associated with the in-grade strength of the timber and when modelling is undertaken up to the clear strength of the wood are shown in Figs. 14 and 15, respectively. A good indication of the behaviour is achieved between the experimental results and the results for the finite element model when using the in-grade strength. Failure of Strain Gauge 1 (SG1), which was located at midspan in the top lamination as shown in Fig. 3, occurs at a bending moment of approximately 32 kN m. Significant nonlinear behaviour is predicted at this location by the finite element
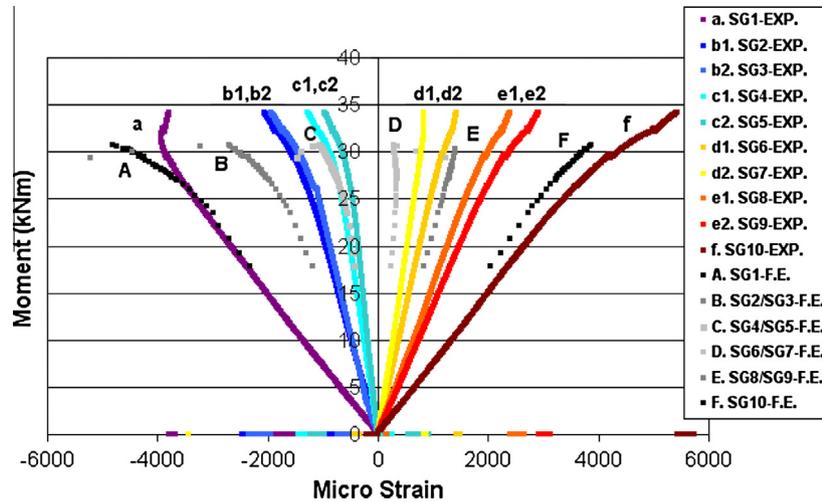
Fig. 14. Phase D: strain profile comparison (Beam 21: in-grade failure).
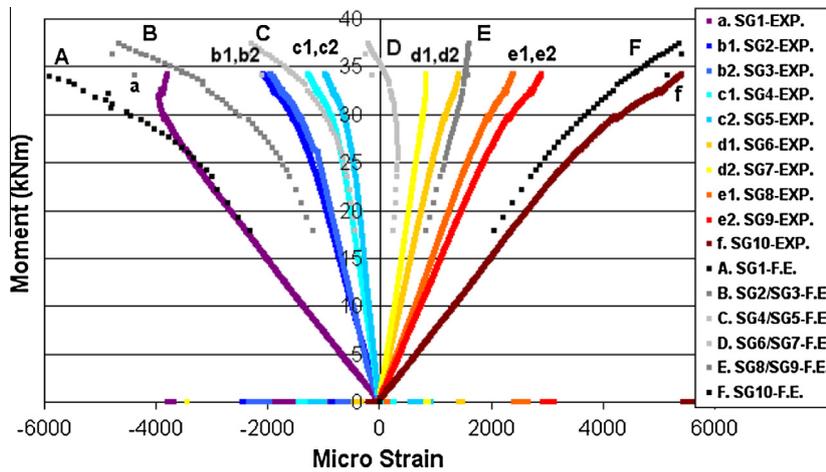

Fig. 15. Phase D: strain profile comparison (Beam 21: tension failure associated with clear wood).

model after the gauge has failed as shown by "A" in Fig. 14. The deviation that exists between the numerically predicted behaviour and the experimental behaviour is as a result of a mean global Young's modulus being used for each entire lamination in comparison to the experimental measurements which were recorded from strain gauges located at midspan. In reality each lamination is non-homogeneous and the material properties will vary throughout. It is seen in Fig. 15 that if the quality of the bottom lamination is improved, extensive nonlinear behaviour is introduced in the compression region of the beam as indicated by "A" and "B". Nonlinear behaviour is also associated with the tensile region as a result of micro-cracking in the beam and this behaviour is also simulated by the finite element model.

4.5. Effect of reinforcement percentage

The modelling work has demonstrated that the behaviour of the experimentally tested beams can be predicted with good accuracy. It is therefore considered appropriate that the model can be used to undertake parametric analyses to determine the influence of increasing reinforcement percentages in the hybrid system. The effect of increasing the reinforcement percentage at the soffit of the Phase B beams and introducing additional nonlinear load–deflection behaviour into the hybrid system is illustrated in Figs. 16

and 17. The load–deflection behaviour determined from failure at the tensile strength associated with the greatest KAR in the timber is illustrated in Fig. 16 and the load–deflection behaviour predicted by failure up to the clear wood of the bottom lamination is shown in Fig. 17. All simulations are carried out for an FRP with a modulus of elasticity of 38,440 N/mm^2, as determined by the material characterisation tests. The behaviour of an unreinforced beam is also shown. The degree of nonlinear behaviour introduced was seen
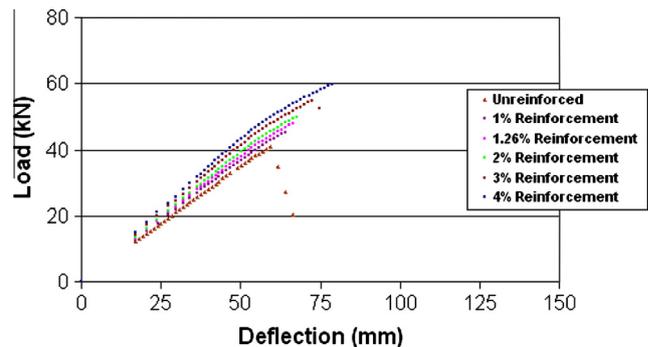

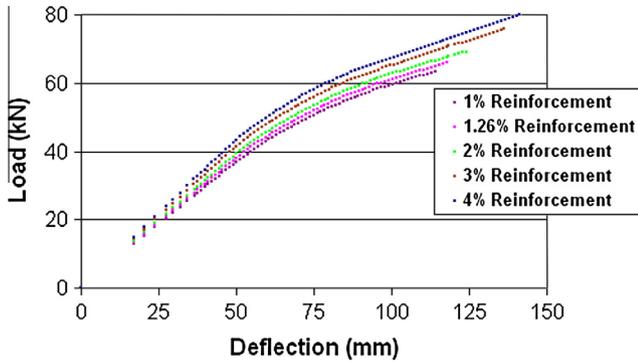**Fig. 16.** Phase B: influence of reinforcement percentage on load–deflection behaviour with in-grade failure.

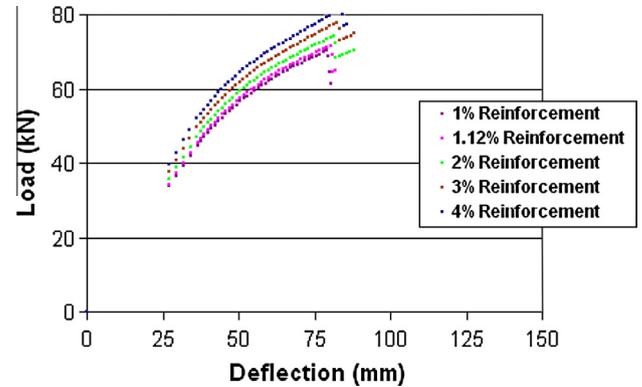**Fig. 17.** Phase B: influence of reinforcement percentage on load–deflection behaviour with clear wood failure.

Fig. 19. Phase D: influence of reinforcement percentage on load–deflection behaviour with clear wood failure.
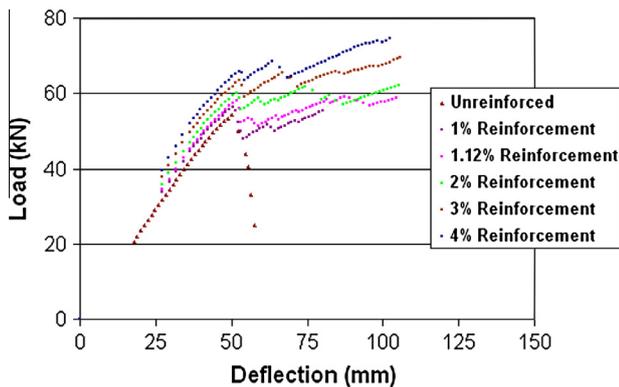

Fig. 18. Phase D: influence of reinforcement percentage on load–deflection behaviour with in-grade failure.

to be highly dependent on the strength of the most extremely stressed tension lamination. Significant enhancements in the stiffness and ultimate moment capacity of the section can also be obtained. Enhancements in stiffness in comparison to an unreinforced beam are predicted to range from 6.6% for 1% FRP reinforcement to 29% for 4% reinforcement. Significantly greater improvements are predicted to occur with regard to the ultimate moment capacity in comparison to an unreinforced section with an improvement of 14.1% predicted for 1% reinforcement and 54.9% predicted for 4% reinforcement. If the strength reducing effects of knots are eliminated in the tension zone, it is predicted that with 1% reinforcement strategically placed at the soffit of Beam 18, an increase of 57.5% would result for the ultimate moment capacity with up to an increase of 116.7% being obtained when using 4% reinforcement.

An examination of the effect that reinforcement percentage had on beams which included a sacrificial laminations was also undertaken. The predicted load–deflection behaviour that is associated with tensile failure initiating at the in-grade strength value for Beam 21 is shown in Fig. 18. The predicted response when failure occurs at a tensile strength of the clear wood is shown in Fig. 19. As was seen with the parametric study for the Phase B beams, increased ductility is achieved as the reinforcement percentage is increased. Significant ductility is predicted post fracturing of the sacrificial lamination. Increased ductility is also particularly evident if the strength of the sacrificial lamination is improved. This could be achieved by using finger-joints to eliminate defects. For plate reinforcement percentages of 1% and 4%, improvement in stiffness of 6.1% and 25.1%, respectively, are predicted in comparison to the performance achieved by an unreinforced glulam beam

associated with identical geometrical characteristics and mechanical properties. Improvements, though favourable, were not of the same magnitude as that with the Phase B beams, as the reinforcement was located above the most highly stressed fibres in the sacrificial lamination. It is envisaged that in commercial production, larger sized reinforced glulam beams would be produced and if FRP plate was strategically positioned above the sacrificial lamination, the distance from the FRP plate to the neutral axis would be much greater and hence the stiffness of the section would be improved. When failure predictions are undertaken to determine the increase in ultimate moment capacity that can be achieved at the in-grade strengths, it is seen that the model predicts an increase of 6.6% with just 1% reinforcement and up to 39.1% with 4% reinforcement. However, it should be noted that the prediction of the model is conservative as the capability of the FRP reinforcement to transfer stresses from weaker locations in the timber and act as a bridge over defects such as knots is not included in the model. Considerably greater enhancements in ultimate moment capacity can be achieved if strength reducing defects are removed from the more highly stressed laminations as shown by the results plotted in Fig. 19.

5. Conclusions

This paper discusses the development of a nonlinear finite element model that has the capability to predict the mechanical behaviour of low-grade glued laminated timber reinforced in flexure with FRP plate material. The model incorporates anisotropic plasticity theory for the timber laminations in the compression zone of the glulam and uses experimental test results and known relationships from the literature as input data. The failure model is based on the maximum stress criterion. The following conclusions are made:

- Strong agreement is found between the simulated load–deflection behaviour and the experimental results of unreinforced and FRP plate reinforced glulam. The model predicts the nonlinear performance of the reinforced beams with good accuracy. Satisfactory results are achieved in relation to the predictions for elastic stiffness and ultimate moment capacity. The results of the simulations appear to suggest that the FRP acts as a bridge over weak defects in the timber thus increasing the performance of the timber with regard to both the stiffness and the ultimate moment capacity of the beam.
- The quality of the most extremely stressed tensile lamination was important in relation to the amount of nonlinear behaviour experienced by the reinforced beams.

- The model can be used to obtain a good indication of the strain profile distribution. It was also seen from the strain profile distributions that as the quality of the most extremely stressed tensile lamination is enhanced, greater plasticity is experienced in the top lamination of the beam.
- The model can act as a useful tool to optimise the system in relation to loading configurations, geometric arrangements, lamination lay-up and quality, mechanical properties of the reinforcement and reinforcement percentage. This has been illustrated by undertaking parameter studies to investigate the influence of the strength properties of the tension laminations and the reinforcement percentage on the structural performance of reinforced beams.

Acknowledgments

References

[1] Hollaway LC, Teng JG. Strengthening and rehabilitation of civil infrastructures using fibre-reinforced polymer (FRP composites). Woodhead Publishing Ltd.; 2008.
[2] Bank LC. Composites for construction: structural design with FRP Materials. John Wiley & Sons; 2006.
[3] Thelandersson S, Larsen HJ. Timber engineering. London: Wiley & Sons; 2003.
[4] Dinwoodie JM. Timber: its nature and behaviour. 2nd ed. Taylor and Francis; 2000.
[5] Raftery G, Harte A. Low-grade glued laminated timber reinforced with FRP plate. Compos Part B: Eng. 2011;42(4):724–35.
[6] Raftery G. The use of advanced composite materials in the flexural reinforcement of low-grade glulam. PhD thesis, Civil Engineering, College of engineering and informatics, National University of Ireland, Galway; 2010.
[7] Tingley DA. The stress–strain relationships in wood and fiber-reinforced plastic laminae of reinforced glue laminated wood beams, Ph.D. Thesis, Oregon State University, Corvallis, OR; 1996.
[8] Kirlin CP. Experimental and finite-element analysis of stress distributions near the end of reinforcement in partially reinforced glulam. MSc. Thesis, Oregon State University; 1996.
[9] Serrano E. Glued in rods for timber structures – a 3D model and finite element parameter studies Int. J Adhes Adhes 2001;21:115–7.
[10] Kasal B, Heiduschke A. Radial reinforcement of curved glue laminated wood beams with composite materials. Forest Prod J 2004;54(1):74–9.
[11] Guan ZW, Rodd PD, Pope DJ. Study of glulam beams prestressed with pultruded GRP. Comput Struct 2005;83(28–30):2476–87.
[12] Alam P. The reinforcement of timber for structural applications and repair, PhD thesis, Dept Mech Eng University of Bath; 2004.
[13] Kim YJ, Harries KA. Modeling of timber beams strengthened with various CFRP composites. Eng Struct 2010;32(10):3225–34.
[14] Valipour HR, Crews K. Efficient finite element modeling of timber beams strengthened with bonded fibre reinforced polymers. Constr Build Mater 2011;25(8):3291–300.
[15] EN 408. Timber structures. Structural timber and glued laminated timber. Determination of some physical and mechanical properties; 1995.
[16] Raftery G, Harte A, Rodd P. Qualification of wood adhesives for structural softwood glulam with large juvenile wood content. J Inst Wood Sci 2008;18(1):24–34.
[17] Raftery G, Harte A, Rodd P. Bond quality at the FRP-wood interface using wood laminating adhesives. Int J Adhes Adhesv 2009;29(2):101–10.
[18] Raftery G, Harte A, Rodd P. Bonding of FRP materials to wood using thin epoxy gluelines. Int J Adhes Adhesv 2009;29(5):580–8.
[19] Raftery G, Harte A. Material characterisation of fast grown plantation spruce. In: Proceedings of the Institution of Civil Engineers, Structures and Buildings; (in press).
[20] ANSYS 5.7 Theory manual.
[21] Hill R. A theory of the yielding and plastic flow of anisotropic metals. Proc Royal Soc A 1949;193:281–97.
[22] Shih CF, Lee D. Further developments in anisotropic plasticity. J Eng Mater Technol 1978;100:294–302.
[23] EN 2747. Glass fibre reinforced plastics – tensile test; 1998.
[24] Zhandarov S, Pisanova E, Mäder E, Nairn JA. Investigation of load transfer between the fiber and the matrix in pull-out tests with fibers having different diameters. J Adhes Sci Technol 2001;15(2):205–22.
[25] Bodig J, Jayne BA. Mechanics of wood and wood composites. Malabar, Florida: Krieger publishing company; 1993.
[26] Falk RH, Colling F. Laminating effects in glued laminated timber beams. J Struct Eng 1995;121(12):1857–63.
[27] EN 338. Structural timber. Strength classes; 2003.